Hindawi Publishing Corporation
International Journal of Aerospace Engineering
Volume 2013, Article ID 284206, 12 pages
http://dx.doi.org/10.1155/2013/284206

Research Article

Development and Validation of a New Boundary Condition for Intake Analysis with Distortion

Foad Mehdi Zadeh, Jean-Yves Trépanier, and Eddy Petro

Department of Mechanichal Engineering, École Polytechnique de Montréal, 2500, Chemin de Polytechnique, Montréal, QC, Canada H3T 1J4

Correspondence should be addressed to Foad Mehdi Zadeh; foad.mehdi-zadeh@polymtl.ca

Received 10 February 2013; Accepted 20 April 2013

Academic Editor: Mark Price

The design of an intake for a gas turbine engine involves CFD-based investigation and experimental assessment in an intake test rig. In both cases, the engine is represented by a mass flux sink, usually positioned a few fan radii aft of the real fan face. In general, this approach is sufficient to analyze intake geometry for low distortion at the fan face, because in this case the interaction of the fan with the inlet flow can be neglected. Where there are higher levels of distortion at the fan face, the interaction could become more significant and a different approach would be preferable. One alternative that takes into account the interaction in such cases includes the fan in the analysis of the intake, using either a steady or unsteady flow model approach. However, this solution is expensive and too computationally intensive to be useful in design mode. The solution proposed in this paper is to implement a new boundary condition at the fan face which better represents the interaction of the fan with the flow in the air intake in the presence of distortion. This boundary condition includes a simplified fan model and a coupling strategy applied between the fan and the inlet. The results obtained with this new boundary condition are compared to full 3D unsteady CFD simulations that include the fan.

1. Introduction

The distortion is defined as a nonuniformity in flow properties as a function of space and time. The spatial flow distortion is usually divided into two types: radial (r), and circumferential (θ). In axial engines, the nonuniform distribution of total pressure associated with an axial velocity deficit is the type of distortion most frequently encountered. In the presence of distortion, the work done by the fan on the flow is nonuniform, and, as a result, the fan influences the distorted upstream flow in an attempt to suppress that distortion. The mass flux sink approach for the boundary condition neglects the interaction between the inlet and the fan, which could be important in operating conditions where the inlet design can result in high levels of distortion or flow recirculation at the fan face. This interaction can be captured using a 3D unsteady approach, where the full 360° fan is included in the inlet analysis. However, this requires significant computational resources. The approach proposed here is to impose a boundary condition on the engine fan face that better represents the interaction of the fan with the distorted flow. This boundary condition consists of a nonuniform static pressure plane which takes into account the effect of the nonuniformity of the work done by the fan blades. For this purpose, the fan is modeled with an Actuator Disc, and the Actuator Disc analysis is coupled with analysis of the flow in the inlet through the theory of parallel compressors. With this process, an improved boundary condition is defined on the fan face under distortion.

This paper is organized as follows: in Section 2, the pertinent literature on the interaction of fans with distortion is reviewed. Then, in Section 3, the selected simplified fan model is presented, which is a variant of the Actuator Disc model. In Section 4, the coupling methodology used to iteratively define the boundary condition on the fan face using both the Actuator Disc model and the theory of parallel compressors is described. Validation of the approach on the NASA Rotor 67 case, as described by Fidalgo et al. [1], is also presented in this section. Finally, in Section 5, an application for a nacelle at high incidence is given.

2. Fan Modeling under Distortion

The simplest approach to modeling a fan subjected to distortion forces is the theory of parallel compressors. This theory models a compressor running under circumferential total pressure distortion [2]. Two separate compressors work on the flow, one on the clean flow and one on the distorted flow, without any interaction. Their operational characteristics are the same, and they both exhaust the flow at a single static pressure, which is the same as the pressure obtained without distortion for the same total mass flow. Experimental tests [3] have confirmed this theory, and other researchers have subsequently improved and validated it [4, 5].

With the development of CFD, researchers investigate distortion using this tool using simplified models of rotating machines. Whiteld and Jameson [6] and Dang [7] described propeller/airframe interaction using analytical source terms and Actuator Disc in computational model, respectively. An affordable CFD approach for modeling turbomachinery is the Streamline Curvature method using body forces or energy sources as the effective elements of engine. In 2001, Hsiao et al. [8] implemented the body forces in an in-house code to simulate the flow through the NASA stages 35 and 22. In terms of separation due to the high angle of attack, their results were consistent with experimental tests. In 2006, Hale et al. [9] have used it to model the interaction between the fan and upstream distortion. The application involves an F-16 fighter jet. With good accuracy, their work shows a 6% decrease in the overall performance of the compressor caused by distortion.

In 2007, Yao et al. applied a URANS solver to predict the effect of inlet distortion for a two-stage compressor [10]. Their results show the formation of a static pressure distortion caused by the distortion of total pressure. This nonuniformity of static pressure induces a swirl in the flow upstream of the fan. In 2010, Fidalgo et al. did a URANS study of the aerodynamics of the NASA Rotor 67 subjected to a circumferential total pressure distortion imposed on 120° at entrance [1]. They also showed the presence of an induced swirl flow at the fan face resulting from the capacity of the fan to redistribute the mass flow in an attempt to suppress distortion.

Although the URANS approach provided detailed and very instructive information about these flows, the high CPU requirements of the approach make its use in design mode prohibitively costly. For practical purposes, it would be useful to have a simplified fan model, which could be embedded in the outflow boundary condition located on the fan face, in order to use CFD for inlet design. The main objective of this paper is to develop such a boundary condition to represent the interaction of the fan with the flow in the intake. According to several of the documents cited above, the work of the fan is not uniform in the case of upstream distortion, and the boundary condition must take this nonuniformity into account. So, our approach will be to devise a simplified fan model and to establish a proper methodology for coupling it with a CFD analysis of the inlet. In the next section, the simplified fan model used in our methodology is presented.

3. A Simplified Fan Model

Of the many aerodynamic fan models available, the Actuator Disc is a fast and cost-effective approach that takes into account the radial distribution of flow properties. It is a mathematical model which considers the fan as a plane comprising an infinite number of blades. This plane induces a discontinuity of tangential velocity.

In 1995, Lewis [11] proposed (1) relating the upstream and downstream axial velocities to their values at the fan boundaries:

$$V_z = V_{z1} + \frac{\left(\rho_2 V_{z2} - \rho_1 V_{z1}\right)}{\rho_m} \frac{e^{kz/(r_t - r_h)}}{2}, \quad z < 0,$$
$$V_z = V_{z2} - \frac{\left(\rho_2 V_{z2} - \rho_1 V_{z1}\right)}{\rho_m} \frac{e^{-kz/(r_t - r_h)}}{2}, \quad z > 0. \tag{1}$$

In (1), V_z is the axial velocity component, ρ is the density, ρ_m is the average density of flows that are the farthest upstream and downstream of the fan, r_t and r_h are the tip and hub radii, respectively, k is a constant related to r_t/r_h, and (1) and (2) represent locations that are the farthest upstream and downstream of the fan, respectively. Note that this version of these equations is applicable to compressible flows.

In order to obtain an equation for the radial variation of V_{z2}, a simplified form of the Navier-Stokes equation is assumed for the fluid elements farthest downstream of the fan and is given by

$$-\frac{1}{\rho}\frac{\partial P}{\partial r} = \left(V_r \frac{\partial V_r}{\partial r} - \frac{V_\theta^2}{r}\right). \tag{2}$$

Then, in (2), one can link pressure to enthalpy via the first law of thermodynamics, use the Euler equations for turbomachinery to relate enthalpy to tangential velocity changes, and relate axial and tangential velocities at the trailing edge of the blade through the velocity triangle. After some tedious manipulations, the final equation for the radial variation of V_{z2} is given by (3). More details about this development can be found in [12]. In (3), velocity components at the trailing edge are related to station 2 using (1):

$$\frac{dV_{z2}}{dr} = \frac{tg^2\beta_2 \left(V_{z,te}/V_{z2}\right)\left(\left(F/\rho_m\right)\left(d\rho_2/dr\right) + \left(d\rho_2/dr\right)\left(\rho_2 F/2\rho_m^2\right)\right)V_{z2}}{1 + tg^2\beta_2 \left(V_{z,te}/V_{z2}\right)\left(1 - \left(\rho_2/\rho_m\right)F\right)}$$
$$+ \frac{tg^2\beta_2 \left(V_{z,te}/V_{z,2}\right)\left(d\rho_2/dr\right)\left(\rho_1 F/2\rho_m^2\right)V_{z1}}{1 + tg^2\beta_2 \left(V_{z,te}/V_{z2}\right)\left(1 - \left(\rho_2/\rho_m\right)F\right)}$$

$$+\frac{2\omega r\left(V_{z,te}tg\beta_2/V_{z2}r\right)-V_{z,te}tg\beta_2\left(V_{z,te}tg\beta_2/V_{z2}r\right)}{1+tg^2\beta_2\left(V_{z,te}/V_{z2}\right)\left(1-\left(\rho_2/\rho_m\right)F\right)}$$

$$-\frac{V_{z,te}r\left(d\left(tg\beta_2\right)/dr\right)\left(V_{z,te}tg\beta_2/V_{z2}r\right)}{1+tg^2\beta_2\left(V_{z,te}/V_{z2}\right)\left(1-\left(\rho_2/\rho_m\right)F\right)}, \tag{3}$$

with

$$F=\frac{1}{2}e^{-kz/(r_t-r_h)}. \tag{4}$$

In this equation, the density at the downstream location is linked to the upstream density value with an additional equation for the global fan efficiency. Integrating (3) with the constraint of respecting mass conservation enables us to obtain the radial distribution of the axial velocity at the location farthest downstream. Using these values and classical thermodynamic relations, all the other flow properties can be obtained.

With this Actuator Disc model, the flow analysis can be performed to relate the upstream and downstream locations of the fan.

The input data for this model are:

(i) blade trailing edge angle versus radial direction: $\beta_2(r)$,

(ii) fan speed: ω,

(iii) total pressure and temperature at the location farthest upstream: P_t and T_t,

(iv) flow rate: $\dot{m}$,

(v) polytropic efficiency: η.

To validate this model, an incompressible rotor presented by Lewis [13] is used. Figure 1 presents the velocity profiles along the trailing edge and at the farthest location downstream for comparison purposes. All these results are consistent with those presented by Lewis.

4. Fan and Upstream Flow Coupling

4.1. Work and Distortion. A simple analysis can be performed to illustrate the effect of distortion on the fan's work. This work on different stream tubes of a distorted flow is not uniform, mainly owing to different flow rates. To illustrate this effect, velocity triangles can be drawn for both the clean and distorted parts, as in Figure 2, where U is the rotational speed and $V_{\theta 2}$ is the swirl velocity at the exit of the blade.

One can see that a reduced mass flow results in an increase in tangential velocity at the outlet, which leads to increased work. This shifts the local operating point of the fan, and the ratio of total pressure for the distorted streamlines is higher than that for the clean part, as illustrated on the compressor map given in Figure 3.

4.2. Development of an Iterative Method to Define the Boundary Condition. A case study from Fidalgo et al. [1] is used. A sketch of their geometry is given in Figure 4. Their work is aimed at determining the nature of the interaction between NASA Rotor 67 and the flow under distortion. As shown in Figure 4, the air intake includes a cylindrical channel and a round-shaped nose in front of the fan face, identified as LE. In Figure 4, the numbers 1, 2, and 3 identify reference planes on which the flow properties are calculated for comparison purposes. The flow distortion is imposed in a circumferential zone (120°) on the inlet plane as a reduced total pressure.

The proposed boundary condition is placed on the fan face, LE. This plane is then divided into sectors, so as to impose a different boundary condition in each sector. In this study, simulations with 12 uniformly distributed radial sectors, as shown in Figure 5, are used.

4.3. Coupling of the Actuator Disc and CFD Solver. The Actuator Disc model and the intake CFD model are coupled using the theory of parallel compressors. Based on this theory, the average static pressure for all the stream tubes exhausting at the farthest location downstream of the fan has to be equal to the static pressure for the case without distortion. In order to implement this theory, an iterative approach is used, which is summarized as follows.

(i) Run a CFD simulation of the intake by imposing a uniform static pressure plane on the intake's outflow plane (corresponding to the fan face, LE). Adjust the static pressure to match the required total mass flow. For each sector, compute the average flow rate and swirl angle and send these as input to the AD program.

(ii) Run the AD program for every sector independently.

(iii) Calculate the average static pressure profile at the location farthest downstream.

(iv) Compare the average static pressure profile with the static pressure profile obtained with a uniform flow distribution (clean).

(v) Apply an iterative process to eliminate the gap between the two static pressure profiles (average and clean) by varying the static pressure for each sector.

4.4. The Iterative Process. As discussed previously, the main effect of the fan on the distorted upstream flow is to suck the regions of low mass flow more strongly. This nonuniform suction redistributes the flow on the inlet plane, an effect which is obtained by imposing a lower static pressure on the sectors having low mass flow. Our convergence criterion involves a comparison of the average static pressure profile at the farthest downstream location with the same profile

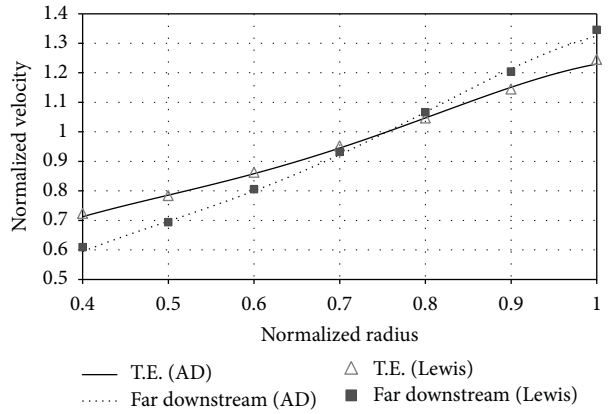

Figure 1: Velocity profiles.

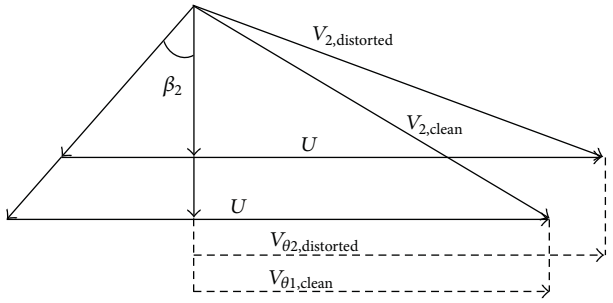

Figure 2: Velocity triangles.

without distortion. To achieve this, an iterative process is defined using

$$\frac{P_i^{n+1}}{\overline{P}} = 1 + \alpha^{n+1}\left(\frac{\dot{m}_i^n}{\overline{m}} - 1\right). \tag{5}$$

In (5), the value of the static pressure for each sector (i) is redefined as a function of its flow rate at the previous iteration (n) multiplied by a factor α, which is based on the difference between the average static pressure profile and the static pressure profile obtained without distortion. According to (5), the static pressure is reduced in areas with a flow deficit and increased in areas with extra flow. This tends to balance the mass distribution. The parameter value (α) is determined using the secant method, as given by

$$\alpha^{n+1} = \alpha^n - \frac{\Delta P^n}{\Delta P'^n}, \qquad \Delta P'^n = \frac{\Delta P^{n-1} - \Delta P^n}{\alpha^{n-1} - \alpha^n}. \tag{6}$$

The mass flow rate and the static pressure distributions corresponding to the first and last iterations are reproduced in Figure 6. One can see that the iterative process has decreased the pressure in the distorted region, and, as a result, the flow rate has increased in that region.

To determine the adequate mesh size, a grid independence study was done, as presented in Figure 7. RMS

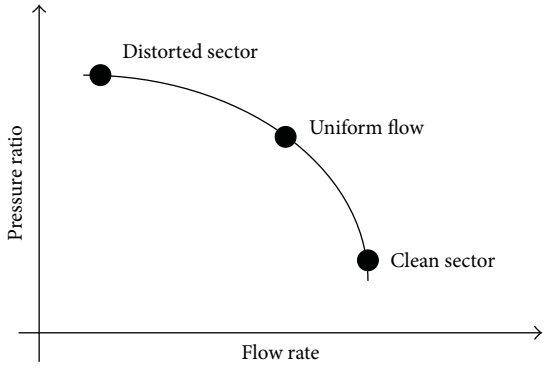

Figure 3: Local operation points.

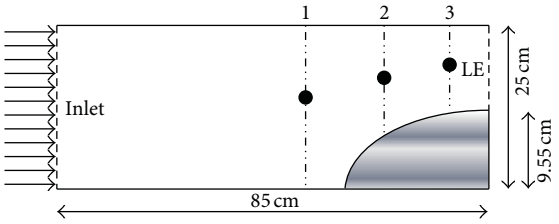

Figure 4: Air duct and reference planes.

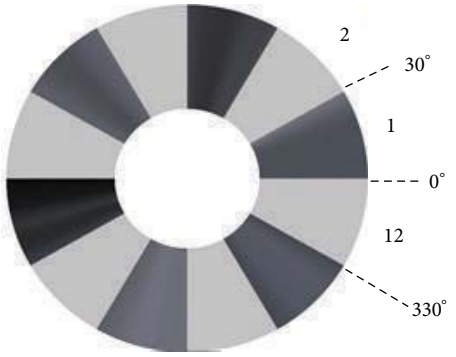

Figure 5: Divided sectors.

difference of the normalized variable, ρV_z, was employed as the accuracy criterion. A mesh composed of 78000 nodes is selected to perform the simulations using the standard k-epsilon turbulence model with a scalable wall treatment. As it was shown in Figure 7, above the vicinity of this node number, simulation's accuracy remains in the same order of magnitude with less than 1% of difference. It should be noted that these values are obtained in comparison with a reference grid of 167736 nodes.

4.5. Results, Validations, and Analysis. In this section, our results are compared to the URANS results from Fidalgo et al. [1]. In Figure 8, the local fan pressure ratio computed for the twelve sectors is shown. One can notice the higher pressure ratios for the distorted sectors and note the fact that the orbits are distributed around the fan speed line. However, the amplitudes of the pressure ratio around the

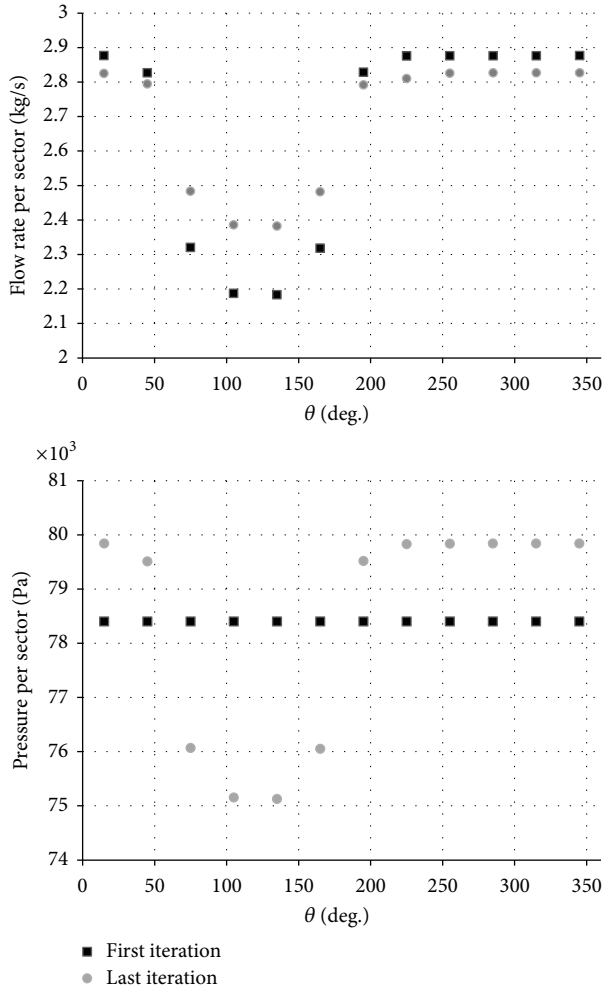

Figure 6: Static pressure and flow rate distribution in the first and last iterations.

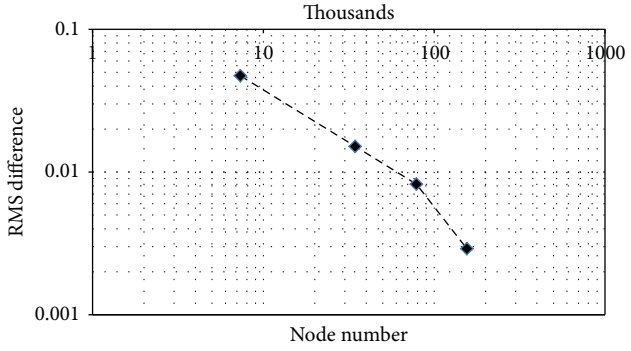

Figure 7: Mesh independence study.

orbits are not the same. These differences are caused by the various assumptions used in our AD-based approach, including that of a constant area flow path across the fan and a constant efficiency. Nevertheless, the qualitative behavior of the circumferential pressure ratio distribution is reproduced well, which should enable us to better represent the effect

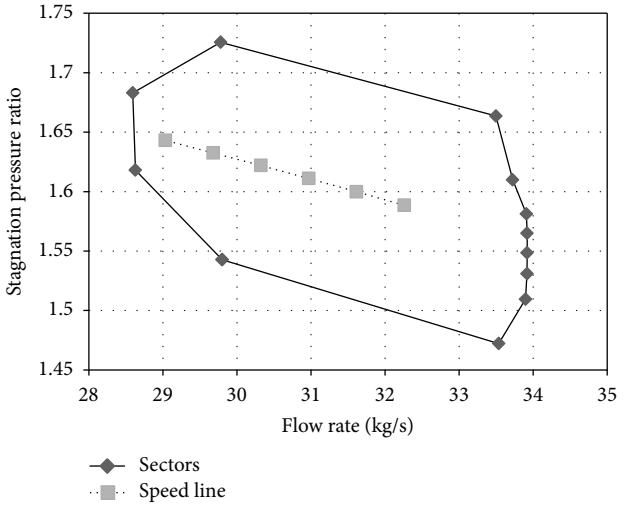

Figure 8: Total pressure ratio of clean and distorted sectors and the speed line.

of the fan on the upstream flow. This will be shown in the following.

Figures 9 to 11 show the circumferential distribution of various properties upstream of the fan on three planes, located at $-0.5C$, $-2.5C$, and $-5.5C$, where C is the axial chord length at the mid-point of the blade (see Figure 4).

On these three planes, three properties are compared:

(i) unit mass flow rate, normalized by the same property at the $-5.5C$ plane for a clean flow;

(ii) static pressure, normalized by the average total pressure at the inlet;

(iii) angle between the absolute velocity vector and the axial direction.

Figure 9 presents the distribution of the unit mass flow rate. According to this figure, the fan attempts to suppress the velocity deficit, and the flow velocity becomes more uniform when the flow approaches the fan face. The AD model results show slightly less distortion than those of Fidalgo et al. [1], but the prediction of the distortion suppression by the two models is similar. The same effect can be observed on the pressure field, as shown in Figure 10. One can see that, in the segments under distortion, the static pressure decreases as the flow approaches the fan. This variation is also well captured by our AD-based boundary condition. Finally, the nonuniform static pressure distribution causes secondary flows upstream of the fan. Figure 11 shows the angle between the velocity vector and the axial direction. One can see that the norm of this angle is maximal at the beginning and at the end of the distortion zone and that its amplitude increases as the flow approaches the fan face. For that property, the agreement between our approach and the URANS results is excellent. Furthermore, a comparison with the experimental results, also provided by Fidalgo et al. at the $-2.5C$ plane, also shows excellent agreement.

The conclusion from this validation is that our AD-based approach for the boundary condition at the fan face

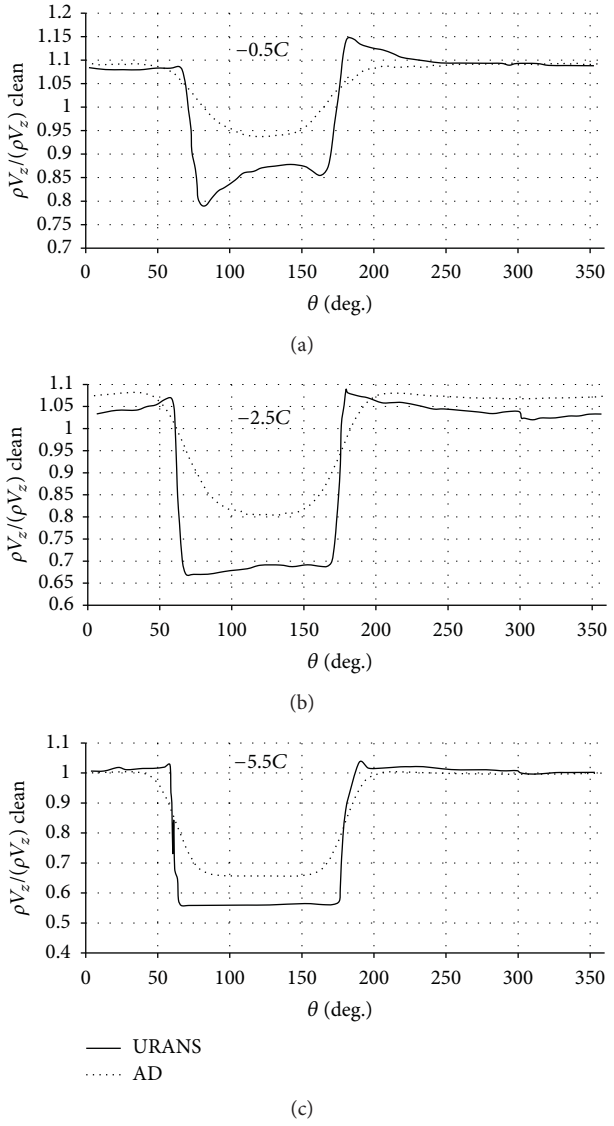

Figure 9: Comparison of unit mass flow rate for 3 reference planes.

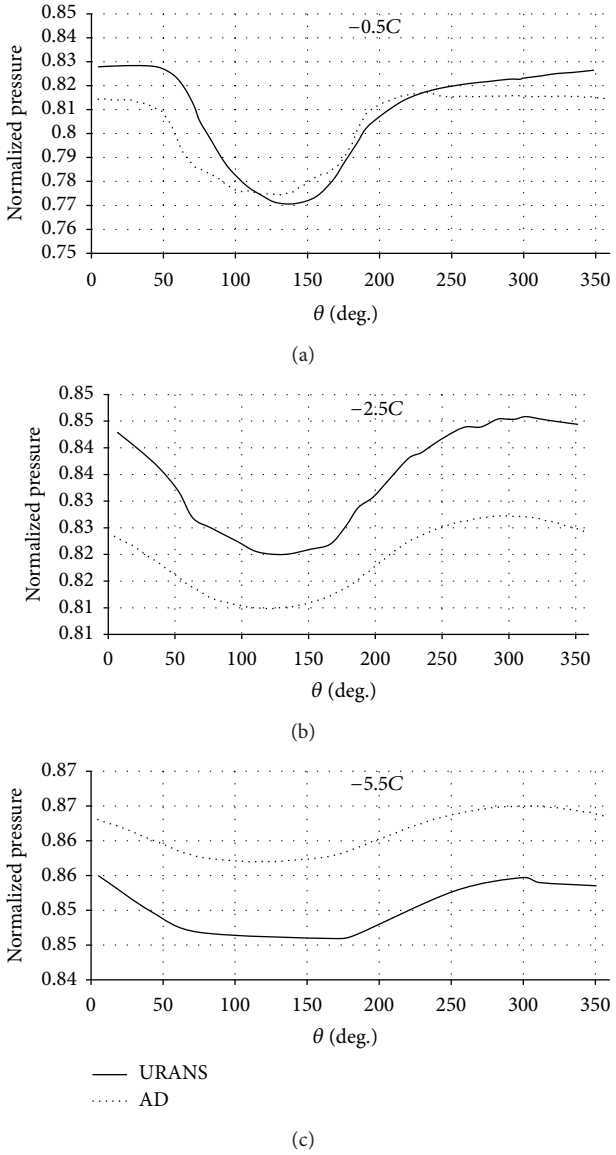

Figure 10: Comparison of the static pressure for 3 reference planes.

provides a good representation of the main characteristics of the interaction of the fan with the inlet flow. As such, it constitutes an improvement over the classical mass flux sink approach. The method is now ready to be applied to a more complex case.

5. A Nacelle at High Incidence

A typical situation to which the developed method could be applied is the study of a nacelle at high incidence. In this case, one would like to be able to predict the onset of flow separation in the inlet as the flow angle increases. However, the interaction of the fan and the inlet can influence the flow separation behavior. In this section, the proposed AD approach is applied and compared to various CFD approaches, obtained with different types of fan and inlet interaction modeling.

5.1. The Geometry and Meshing of the Nacelle Case. The nacelle used in our study here was designed to accommodate NASA Rotor 67. It has a throat diameter of 46.1 cm, which accommodates the rotor; see Figure 12. The nacelle is followed by an ogive-shaped surface 1 meter in length representing the jet flow at the engine exhaust. The nacelle is placed in a rectangular cubic computational domain measuring 41 m × 10 m × 20.7 m, as illustrated in Figure 13.

A partial view of the mesh of the nacelle is shown in Figure 14. The mesh contains 1714560 elements and 1774171 nodes. NASA Rotor 67 can be fitted inside this nacelle. The total mesh, including the nacelle plus the full 22 passage Rotor 67, contains 6254269 elements and 6034624 nodes.

5.2. Aerodynamic Modeling. ANSYS CFX-13.0 was used for all the CFD runs. RANS and URANS models are used

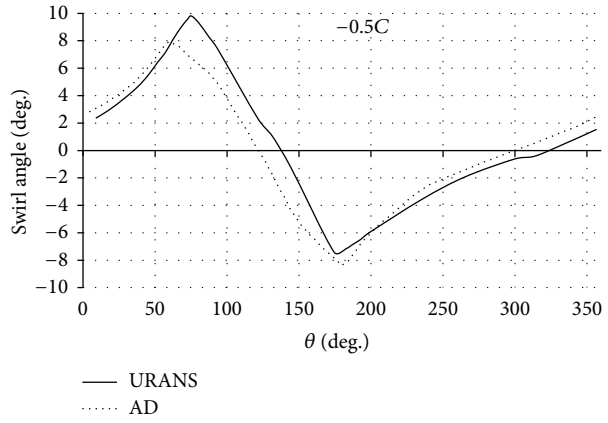

(a)

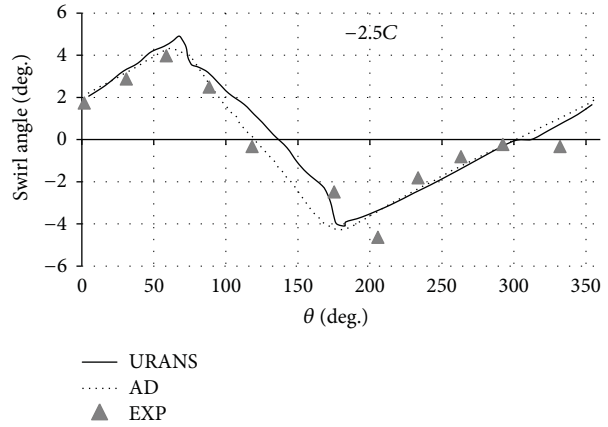

(b)

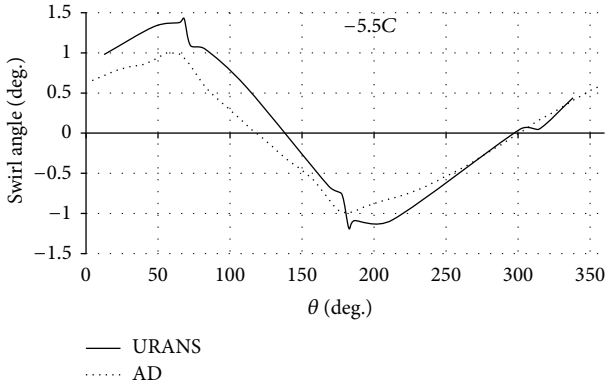

(c)

Figure 11: Comparison of the swirl angle for 3 reference planes.

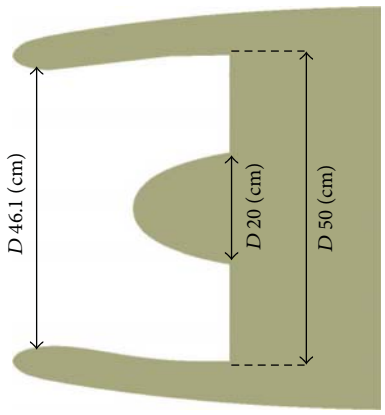

Figure 12: Intake geometry.

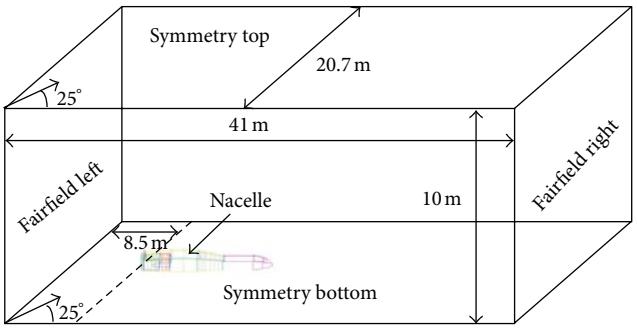

Figure 13: Intake field geometry.

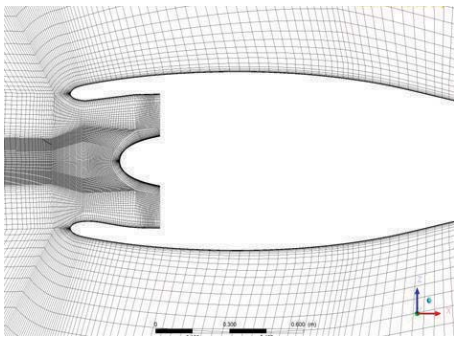

Figure 14: Nacelle meshing.

with the $K\omega$-sst turbulence model. In all cases, the general boundary conditions presented in Table 1 were applied. Note that in order to promote flow separation inside the inlet, the nacelle was placed at a 25° angle of incidence. The mass flow rate imposed in the engine is 33.6 kg/s at 100% of its maximum speed.

Four different approaches to capturing the interaction between the inlet and the fan are compared. The first is the classical mass flux sink approach, where a constant mass flux is imposed on a plane located downstream of the real fan face. The second and third models include the Rotor 67 in the solution: the second model uses the mixing plane approach and seeks a steady state solution of the coupled inlet and single rotor passage domains, and the third model uses URANS modeling of the full 22 Rotor 67 passages inside the nacelle. The fourth model is the AD-based approach currently proposed, where the boundary condition is placed directly on the fan face and the Rotor 67 is absent. In all four simulations, y^+ remains less than 2 on the nacelle's interior

Table 1: General boundary conditions.

Inlet fairfield	Total pressure: 101.325 (kPa) Total temperature: 288.15 (K) Flow direction: 25°
Exit fairfield	Total pressure: 97.7 (kPa)
Nacelle wall and jet surface	No slip

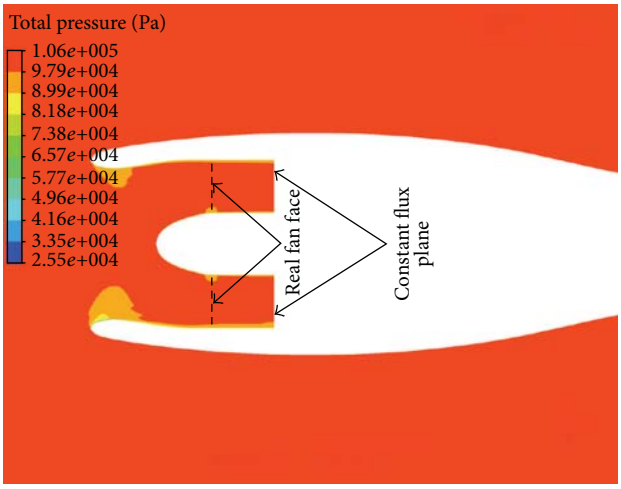

Figure 15: Contours of the total pressure for the constant mass flux model.

wall and less than 25 on the rotor blades. Based on the rotor's diameter, the Reynolds number is 2.5×10^6 and in term of spatial convergence, RMS $\leq 1 \times 10^5$ is guaranteed. The results for these four modeling approaches are presented in the following.

5.2.1. Constant Mass Flux. The first model is the classical mass flux boundary condition. As usual, it is positioned downstream of the real fan face to reduce its influence on the flow in the inlet. In the present run, the mass flux is imposed at 0.2 m behind the fan face, as illustrated in Figure 15. The total pressure contours obtained for this simulation are reproduced in Figure 15. One can observe a small region of lower total pressure on the inside of the lower lip of the nacelle, which is associated with a small separation and reattachment of the flow. With this model, the flow is reattached well ahead of the fan face, and so this simulation predicts only a small flow distortion at the fan face.

5.2.2. Steady State Mixing Plane Approach. To perform the steady state modeling, NASA Rotor 67 is inserted into the nacelle, and a "stage model" interface is placed between the rotor and the inlet. This interface performs a circumferential averaging of the flow properties through the interface. Steady state solutions are then obtained in each frame of reference. Downstream of the rotor, a static pressure is imposed and adjusted to obtain the required flow rate of 33.6 kg/s.

The calculation was performed on 8 2 GHz processors, and 4000 iterations were required to reach convergence. All

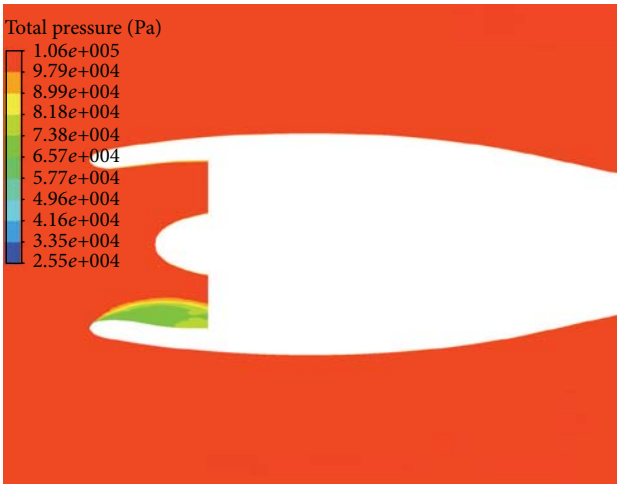

Figure 16: Contours of the total pressure obtained by a steady state calculation.

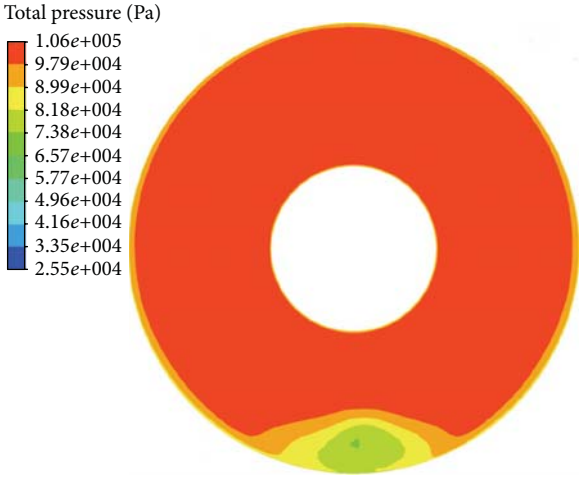

Figure 17: Contours of the total pressure on the fan face obtained by a steady state calculation.

the pressure contours obtained for this simulation are reproduced in Figures 16 and 17. One can observe an important region of separation on the inside of the lower lip of the nacelle, extending to the rotor fan face. As a result of this separation region, the distortion on the fan face is significant with this model. The fact that this result differs substantially from the constant mass flux performed above illustrates the importance of a proper boundary condition for such cases.

5.2.3. Transient Simulation with a Full Rotor. The third model uses URANS modeling with the full 22 passage Rotor 67 inserted into the nacelle. A "transient" interface is used between the rotor and the inlet. This interface transfers information at each time step between the two subdomains and makes it possible to obtain unsteady solutions. This model required much more in terms of CPU resources, as the simulation was performed for 10000 time steps, representing 8 complete revolutions of the fan. Note that periodic behavior

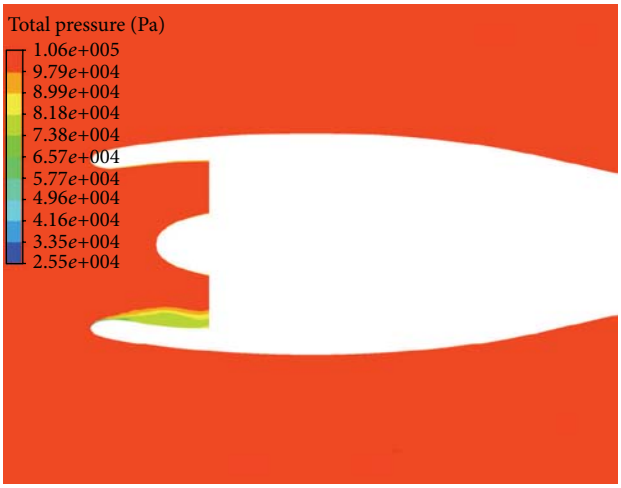

Figure 18: Contours of the total pressure obtained by a transient calculation time step: 600th.

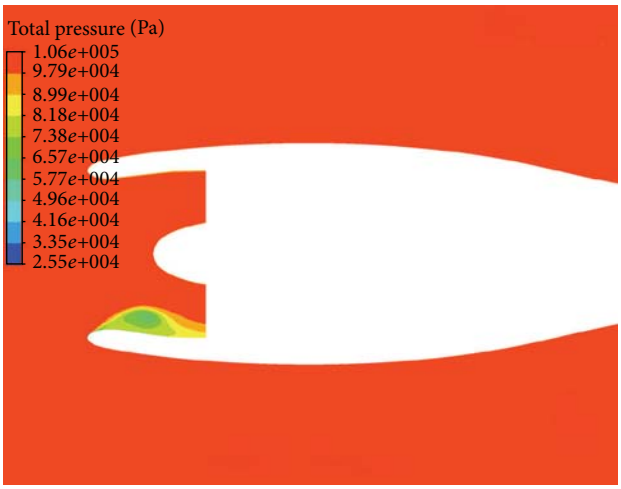

Figure 19: Contours of the total pressure obtained by a transient calculation time step: 2000th.

was reached after 5 revolutions. The calculation was performed on 80 3 Ghz processors and took 2.2 days/revolution. The last 2000 steps were used for reporting the results.

The contours of the total pressure are presented in Figures 18 and 19 for two different time steps. It is obvious that the flow is unsteady, as the size of the flow separation varies in time. Averaged properties are presented in the following and compared to those of the other models.

5.2.4. Actuator Disc Model. The last model used is the AD-based approach proposed in this paper, which imposes our new boundary condition directly on the fan face. Figures 20 and 21 show the contours of the total pressure obtained with the AD-based boundary condition. One can see that the size of the separated region is important and compares well, qualitatively, to those of the steady state and

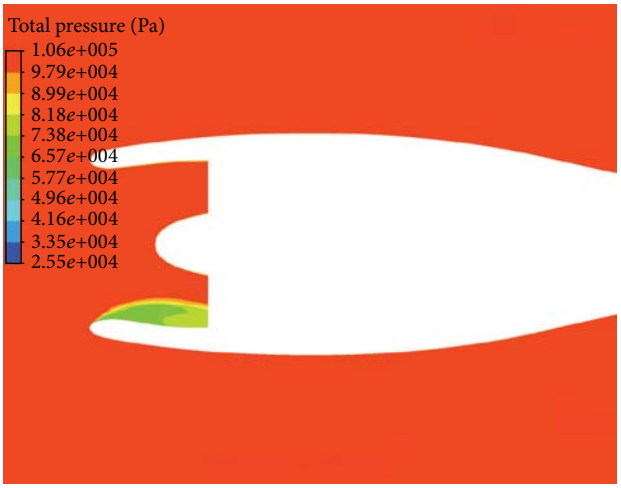

Figure 20: Contours of the total pressure obtained by the AD at the last iteration.

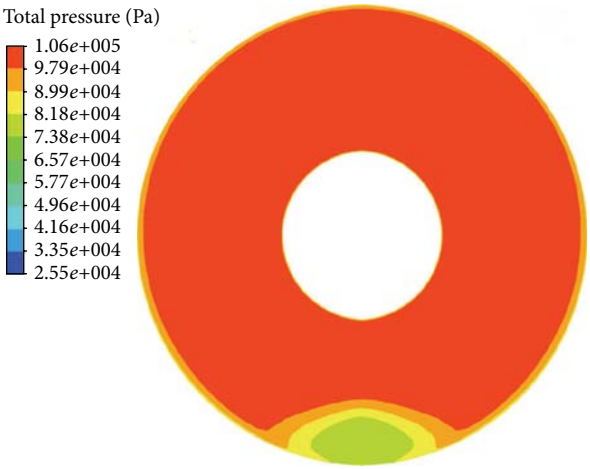

Figure 21: Contours of the total pressure at the fan face obtained by the AD at the last iteration.

unsteady models. More detailed quantitative comparisons are provided in the following.

5.3. Comparison of Models. Our final quantitative comparison of the four models tested involves plotting various flow properties on three different planes upstream of the fan face. The selected planes are the same as those used by Fidalgo et al. [1] and are illustrated in Figure 4. The flow properties compared are also the same as the Fidalgo properties, namely,

(i) axial speed multiplied by density,

(ii) static pressure,

(iii) angle between the absolute velocity vector and the axial direction.

Values are calculated at mid-span of the reference planes, presented in Figure 4 as black points.

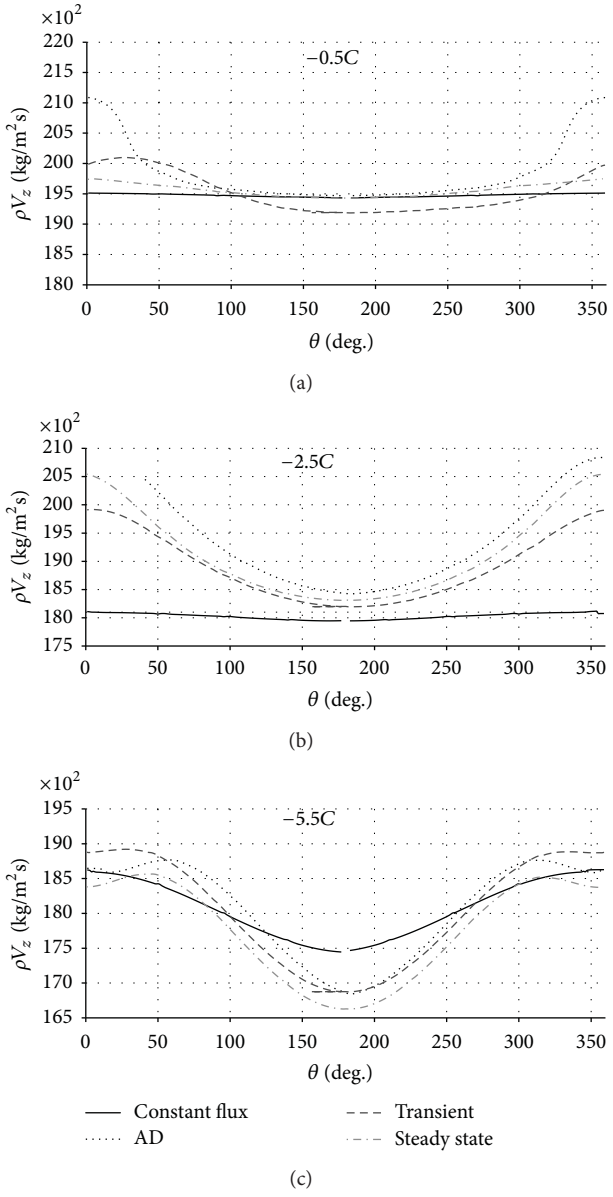

Figure 22: Comparison of unit mass flow rate of the first reference line.

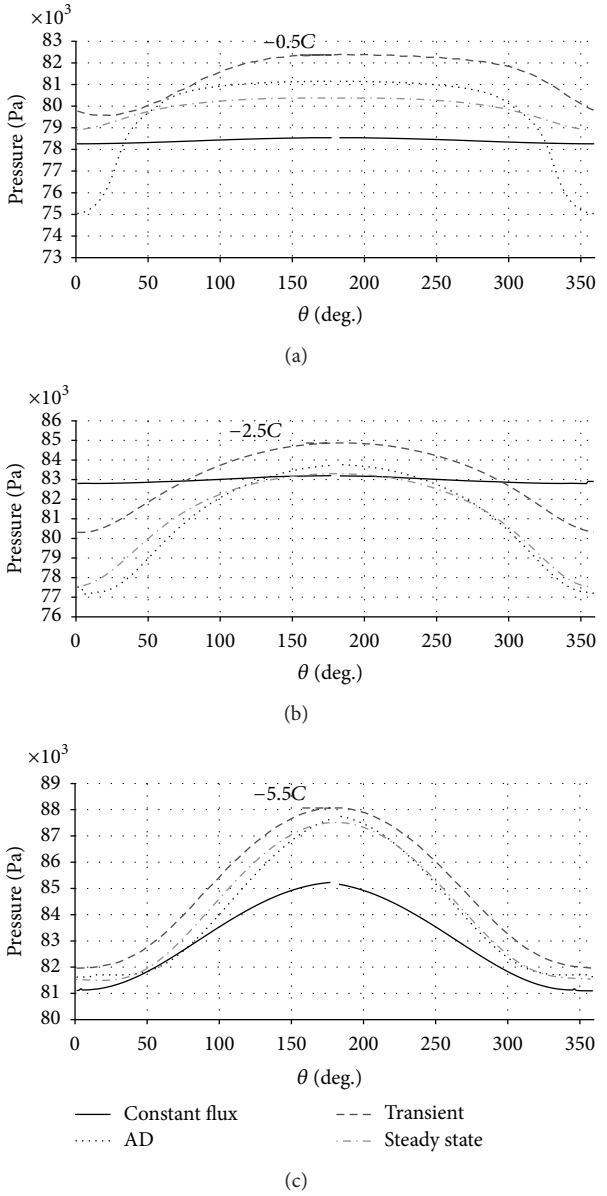

Figure 23: Static pressure comparison.

In these graphs, the transient case reported corresponds to a time average of the flow properties in the 8th revolution of the fan.

Figure 22 illustrates the evolution of unit mass flow rate field as the flow approaches the fan face. One can see that this property becomes more uniform as the flow approaches the fan face, indicating that the fan is attempting to eliminate the distortion. These figures clearly show that the uniform mass flux boundary condition produces the wrong results for the three planes reported. However, the other three models are similar, and the results obtained with the AD-based method are in good agreement with those of the transient and steady state models.

The static pressure profiles corresponding to these distributions are shown in Figure 23. Since the distortion is almost eliminated by imposing a constant flux, the pressure distribution corresponding to this case is almost constant when compared to those of the other models.

Figure 24 illustrates the angle between the velocity vector and the axial direction at the three planes. As expected, the magnitude of this angle is lower for constant flux, because the distortion is almost eliminated.

Overall, one can conclude that the results obtained with the AD-based boundary condition are, in general, close to those of the steady state "stage model" simulation and qualitatively represent the main trends observed in the transient case. Since the AD-based model is the cheapest in terms of CPU requirements, because the rotor is not included in

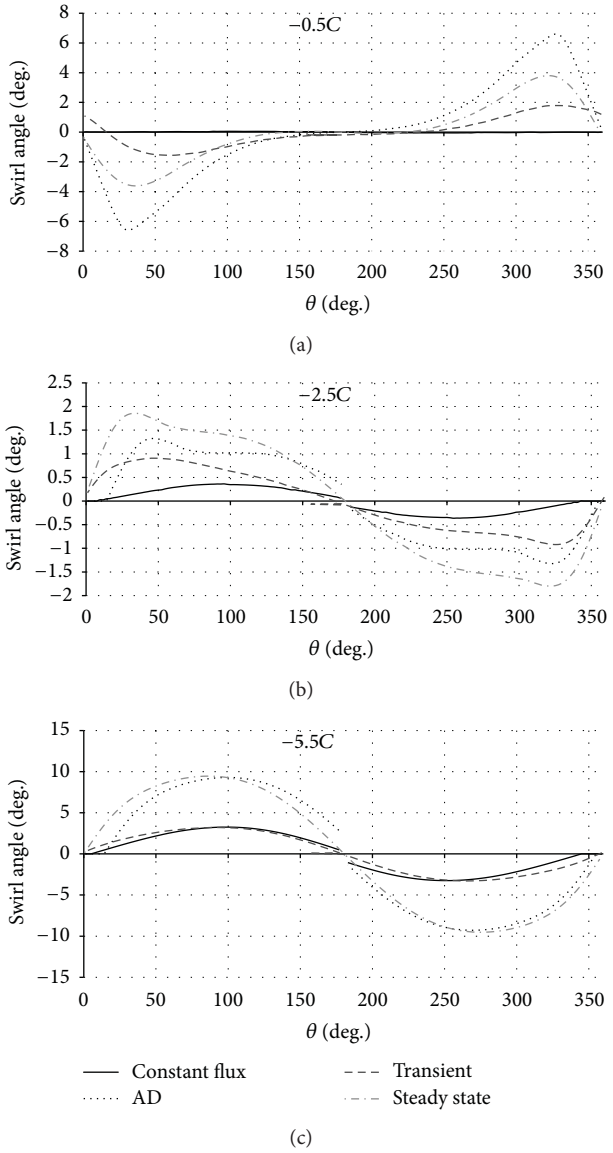

Figure 24: Swirl angle comparison.

the simulation but rather replaced by an AD, the AD-based approach seems to be an interesting compromise for inlet analysis and design.

6. Conclusion

In this work, a boundary condition at the engine fan face has been developed and tested to provide a better representation of the effect of the interaction between the fan and the inlet flows in cases with distortion at the fan face. First, an Actuator Disc model is used as a simplified model of the fan. Next, using the theory of parallel compressors, we divided the fan into several sectors, each of which contains an Actuator Disc. Then, we iteratively adjusted the static pressure in the various sectors of the fan face, in order to match the average outlet static pressure of a flow without distortion. The results obtained by our proposed AD-based approach were compared with the steady and unsteady RANS CFD results for two test cases involving NASA Rotor 67. The proposed AD-based approach gives results that are fairly similar to those of the RANS and URANS models and shows substantial improvement over those of the classical constant mass flux approach.

Nomenclature

a: Axial
AD: Actuator Disc
C: Blade Chord
c_p: Thermal capacity at constant pressure
h: Enthalpy
h_t: Total enthalpy
LE: Leading edge
$\dot{m}$: Mass flow rate
P: Static pressure
P_t: Total pressure
$\overline{P}$: Average static pressure
r: Radial
rel: Relative
RMS: Root mean square
s: Entropy
T: Static temperature
T.E.: Trailing edge
T_t: Total temperature
U: Rotating velocity
V: Absolute velocity
y^+: Dimensionless wall distance
α: Convergence factor
β: Relative angle
η: Efficiency
ω: Rotation
ρ: Density
θ: Angular position.

Acknowledgments

The authors thank Pratt & Whitney Canada, the J.-A. Bombardier Foundation, and the NSERC for their financial support of the IDEA Chair.

References

[1] V. Fidalgo, C. Hall, and Y. Colin, "A study of fan-distortion interaction within the nasa rotor 67 transonic stage," in *ASME Turboexpo Conference*, 2010.

[2] H. Pearson and A. McKenzie, "Wakes in axial compressors," *Journal of the Royal Aeronautical Society*, vol. 63, pp. 415–416, 1959.

[3] C. Reid, "The response of axial flow compressors to intake flow distortion," in *Proceedings of the International Gas Turbine and Aero-Engine Congress and Exhibition*, ASME, New York, NY, USA, 1969.

[4] R. S. Mazzawy, "Multiple segment parallel compressor model for circumferential flow distortion(in jet engines)," *Journal of*

Engineering for Power-Transactions of the ASME, vol. 99, no. 2, pp. 288–296, 1977.

[5] A. H. Stenning, "Inlet distortion effects in axial compressors," *Journal of Fluids Engineering, Transactions of the ASME*, vol. 102, no. 1, pp. 7–13, 1980.

[6] D. L. Whiteld and A. Jameson, "Three-dimensional Euler equation simulation of propeller-wing interaction in transonic flow," in *Proceedings of the 21st American Institute of Aeronautics and Astronautics, Aerospace Sciences Meeting*, Reno, Nev, USA, 1983.

[7] T. Q. Dang, "Calculations of propeller/airframe interference effects using the potential/multienergy flow method," *AIAA journal*, vol. 28, no. 5, pp. 771–777, 1990.

[8] E. Hsiao, M. Naimi, J. P. Lewis, K. Dalbey, Y. Gong, and C. Tan, "Actuator duct model of turbomachinery components for powered-nacelle Navier-Stokes calculations," *Journal of Propulsion and Power*, vol. 17, no. 4, pp. 919–927, 2001.

[9] A. Hale, M. Davis, and J. Sirbaugh, "A numerical simulation capability for analysis of aircraft inlet-engine compatibility," *Journal of Engineering for Gas Turbines and Power*, vol. 128, no. 3, pp. 473–481, 2006.

[10] J. Yao, S. E. Gorrell, and A. R. Wadia, "A time-accurate CFD analysis of inlet distortion induced swirl in multistage fans," in *Proceedings of the 43rd AIAA/ASME/SAE/ASEE Joint Propulsion Conference*, pp. 628–641, July 2007.

[11] R. I. Lewis, "Developments of actuator disc theory for compressible flow through turbo-machines," *International Journal of Mechanical Sciences*, vol. 37, no. 10, pp. 1051–1066, 1995.

[12] F. Mehdi Zadeh, *Amélioration de la Condition Frontière de Face de Soufflante Pour la Conception de L'admission D'Air Sous Distorsion*, École Polytechnique de Montréal, 2011.

[13] R. Lewis, *Turbomachinery Performance Analysis*, vol. 1, Butterworth-Heinemann, 1996.